EUROPEAN ORGANIZATION FOR NUCLEAR RESEARCH

RESPONSE TO ELECTRONS AND PIONS OF THE CALORIMETER FOR THE CHORUS EXPERIMENT

E. Di Capua, M. Ferroni, C. Luppi, S. Ricciardi, B. Saitta[1] and P. Zucchelli
Università di Ferrara and INFN Sezione di Ferrara, Italy

S. Buontempo, A.G. Cocco, A. Ereditato, G. Fiorillo, F. Garufi, F. Marchetti-Stasi, M. Messina, P. Migliozzi, V. Palladino and P. Strolin
Università "Federico II" and INFN Sezione di Napoli, Italy

A. Capone, D. Depedis, U. Dore, P.F. Loverre, D. Macina[2], M.A. Mazzoni, G. Piredda, P. Righini and R. Santacesaria
Università "La Sapienza" and INFN Sezione di Roma, Italy

ABSTRACT

We built and tested on charged particle beams the high energy-resolution calorimeter for the CHORUS experiment, which searches for ν_μ-ν_τ oscillations in the CERN Wide Band Neutrino beam. This calorimeter is longitudinally divided into three sectors: one electromagnetic and two hadronic. The first two upstream sectors are made of lead and plastic scintillating fibers in a volume ratio of 4/1, and they represent the first large-scale application of this technique for combined electromagnetic and hadronic calorimetry. The third sector is made of a sandwich of lead plates and scintillator strips, and complements the measurement of the hadronic energy flow. In this paper, we briefly describe the calorimeter design and show results on its response to electrons and pions, obtained from tests performed at the CERN SPS and PS. An energy resolution of $\sigma(E)/E = (32.3 \pm 2.4)\%/\sqrt{E(\text{GeV})} + (1.4 \pm 0.7)\%$ was achieved for pions, and $\sigma(E)/E = (13.8 \pm 0.9)\%/\sqrt{E(\text{GeV})} + (-0.2 \pm 0.4)\%$ for electrons.

(Submitted to Nuclear Instruments and Methods)

---

[1]Now at Università di Cagliari and Sezione INFN, Cagliari, Italy
[2]Now at CERN, Geneva, Switzerland

1. Introduction

The calorimeter described in this paper, built as a component of the CHORUS detector, is the first large-scale application of the technique of embedding plastic scintillating fibers into a lead matrix, developed over the last few years [1]. The fiber sectors consist of about 1500 km of 1 mm diameter fibers in a lead-to-scintillator volume ratio of 4/1, which allows for compensation and provides good energy resolution in the detection of hadrons. Some of the 414 modules which make up the calorimeter were tested with electron and muon beams prior to installation; the results of these measurements have been previously reported [2]. The whole calorimeter was then tested with electrons, muons and pions.

After a brief description of the calorimeter design and construction, we present here experimental results on the detector response to electrons and pions.

CHORUS started to take data in April 1994 in the CERN Wide Band Neutrino Beam, and the calorimeter operated successfully during the first two years of data taking.

2. Calorimeter design

The CHORUS experiment [3] searches for ν_μ–ν_τ oscillations in the CERN SPS Wide Band Neutrino Beam. It uses nuclear emulsions to directly observe τ decays, produced by charged current interactions of ν_τs, to be extracted out of a large background of ordinary ν_μ interactions. The events to be scanned in the emulsions are selected on the basis of kinematic variables, measured by means of electronic detectors. Such a selection is more efficient if the hadron shower following the neutrino interaction is measured with high angular and energy resolution. In order to detect the τ muonic decay, it is also necessary to efficiently track throughgoing muons in the calorimeter and to match their trajectories with those determined by the other detectors of the apparatus.

A description of the design and construction of the calorimeter for the CHORUS experiment can be found in Ref. [2], where we also present the response of groups of modules to electrons of different momenta. In this paper, we simply outline the main design features, summarized in Table 1. An isometric view of the detector is shown in Fig. 1.

The calorimeter is arranged in elements (modules) to form planes oriented orthogonally to the beam, alternately with horizontal and vertical modules. This structure is mainly motivated by the necessity of providing muon tracking. This is the main difference with respect to the original SPACAL geometry [1], where the modules have fibers parallel to the beam direction and the signals are collected at the back of the calorimeter. The module width orthogonal to the beam is made smaller than the size of the average hadron shower to allow for reconstruction of the hadronic energy flow with sufficient accuracy.

1
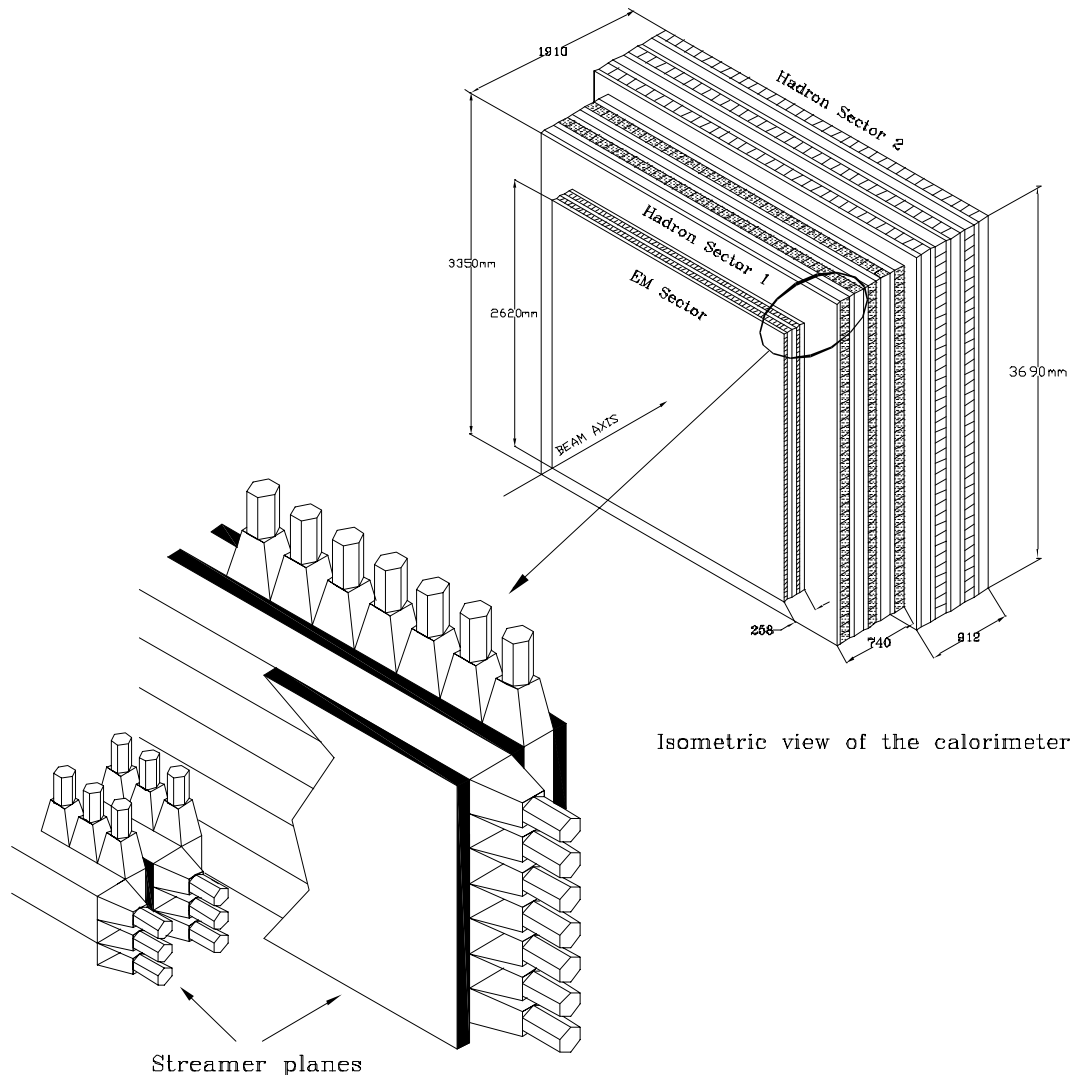
Figure 1: Isometric view of the calorimeter.

The calorimeter consists of three sectors with decreasing granularity (EM, HAD1 and HAD2). The first of these measures the electromagnetic component of the events, while the other two complete the measurement of the hadron showers. The average interaction length [4] of the calorimeter is 21 cm, its radiation length 0.72 cm; the effective Moliere radius is 2 cm and the density of the modules 9 g/cm³. The total calorimeter thickness is about 5.2 interaction lengths (144 radiation lengths), sufficient to contain 99% of the shower induced by a 5 GeV/c pion. It should be noted that about 90% of the hadrons produced in the neutrino interactions have momentum less than 5 GeV/c.

Table 1: Calorimeter design features

	EM	H1	H2	Total
Depth: $X_\circ(\lambda_{\mathrm{int}})$	21.5 (0.78)	55.2 (2.0)	67.1 (2.44)	143.8 (5.22)
Number of planes	4	5	5	14
Number of modules	124	200	90	414
Module dimensions (cm^3)	$4 \times 8 \times 262$	$8 \times 8 \times 335$	$10 \times 20 \times 369$	—
PM per module	4	2	4	—
Total number of PM	496	400	360	1256
PM type	Hamamatsu R1355/SM	Thorn–EMI 9839A	Thorn–EMI 9839A	—
Fiber/strip type	Kuraray SCS-F81	Bicron BCF-12	Bicron BC-408 (strips)	—
Number of fibers/strips	93000	310800	900	—
Total fiber/strip length (km)	283	1165	3	—
Pb weight (tons)	9.7	42	60	111.7

The EM and the HAD1 sectors (2.8 interaction lengths altogether) are made of scintillating fibers and lead, while HAD2 is a sandwich of lead and scintillating strips. The transverse structure of the calorimeter allows light to be collected by photomultipliers (PMs) on both sides of the module, thus reducing the effects of light attenuation in the scintillator [2].

Sets of limited streamer tube planes are inserted between the horizontal and vertical planes for tracking purposes; they are arranged in pairs with horizontal and vertical wires. There are 22 planes, with a total of about 7500 wires read out in digital mode.

3. Module design

Two horizontal and two vertical planes, each of 31 modules, compose the electromagnetic sector EM. Individual modules are built by piling up extruded layers of grooved lead and positioning plastic scintillating fibers in the grooves (Fig. 2).
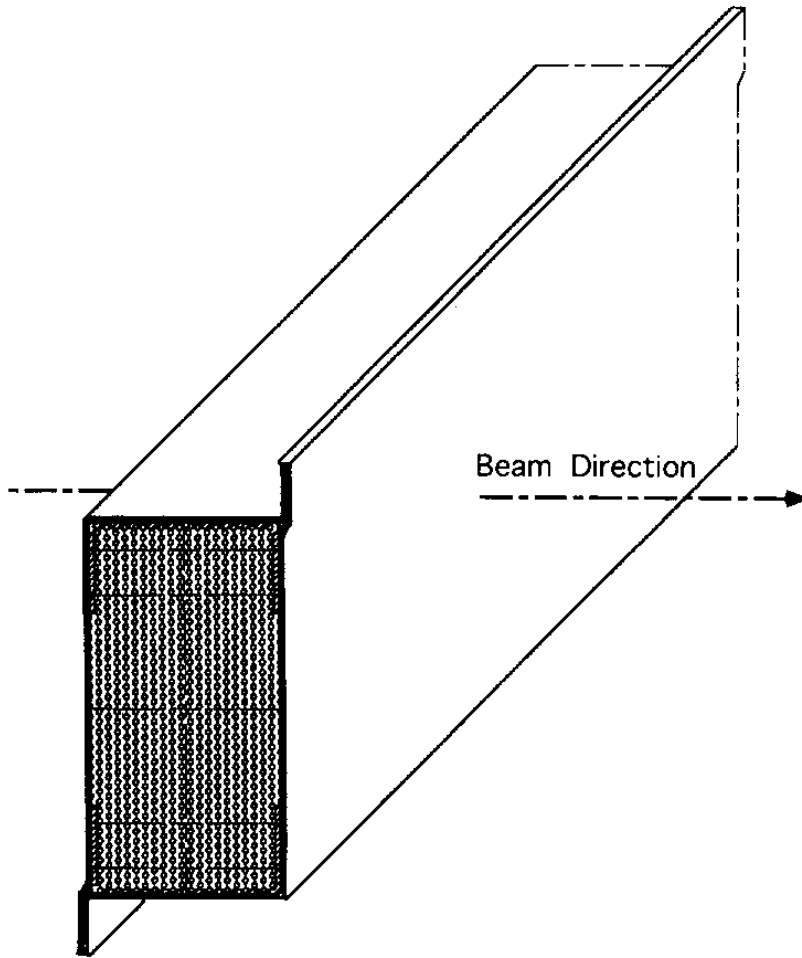
Figure 2: View of an EM module.

The groove diameter is 1.1 mm and the layer thickness 1.9 mm; the material, the same as for the HAD1 and HAD2 modules, is 99% lead and 1% antimony, to improve the mechanical properties. A module consists of a pile of 21 layers, 2620 mm long and 82.4 mm wide, and 740 fibers, each 1 mm in diameter and 3050 mm long. On either side of the module, fibers are assembled in two hexagonal bundles, defining two different read-out cells with about 40×40 mm² cross-section. Each of the fiber bundles is coupled to a 1" PM via a plexiglas light guide. The module is held together by a steel box.

The HAD1 sector consists of 5 planes (3 horizontal and 2 vertical). A plane is formed by 40 modules, each made of 43 extruded layers of lead identical in width and groove size to those used for the EM sector, but with a length of 3350 mm. The

scintillating fibers have 1 mm diameter and 3810 mm length, with a total of 1554 fibers per module. Fibers are collected at both ends in a hexagonal bundle coupled via a light pipe to a 2" PM.

The HAD2 sector also consists of 5 planes (3 vertical and 2 horizontal) with 18 modules each, making a total of 90 modules. Each module is constructed by superposing five alternate layers of one lead bar ($3690 \times 200 \times 16$ mm³) and two adjacent scintillator strips ($3714 \times 100 \times 4$ mm³ each), packed into a stainless steel box open at both ends (Fig. 3).

Figure 3: View of a HAD2 module.

Each of the two groups of five scintillators is coupled to 2" PMs at both ends via plexiglas light guides; therefore, a single module is seen by a total of four PM tubes, and contains two cells.

4. Experimental set-up and data

The main measurements were performed during the autumn of 1993 in the X9 test beam at the CERN SPS. The beam line is almost parallel to the neutrino beam axis. The calorimeter, mounted on rails, can be shifted about four metres sideways from its nominal position to meet the test beam. The set-up is shown in Fig. 4.
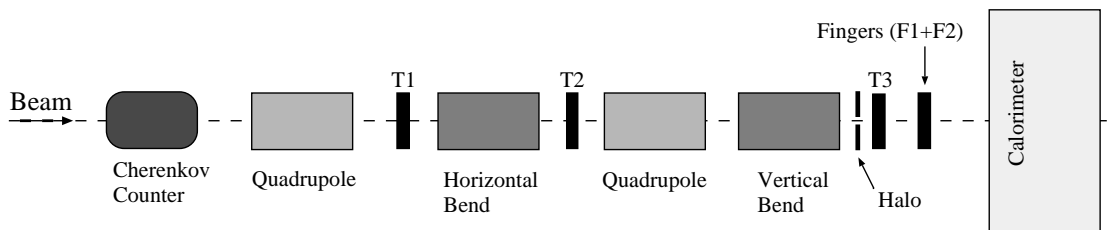
Figure 4: SPS experimental set-up (not to scale).

Coincidences between the scintillation counters $T_1 \cdot T_2 \cdot T_3$ provided the main trigger. The signal from the halo counter was used off-line to reject events initiated upstream of the calorimeter. The particle impact point on the calorimeter was determined by means of the counters F_1 and F_2, each made of four scintillators with dimensions of $1 \times 1 \times 8$ cm³ (fingers), placed orthogonal to the beam line in the horizontal and vertical directions, respectively. In this way, their coincidence defined a matrix of 16 impact regions each of 1 cm².

Electron data were taken from pure beams from 2.5 to 10 GeV/c, while pions originated from mixed electron/pion beams from 3 to 20 GeV/c. A nitrogen Cherenkov counter placed upstream in the beam line gave the electron/pion separation. In the energy interval explored by our measurements, the residual electron contamination of the pion sample was $\sim 2\%$. Muons were rejected off-line by exploiting the unambiguous signature given by the calorimeter itself. Figure 5 shows the features of muon and pion events in a lego plot where the total pulse-height is plotted against the total number of hit PMs.
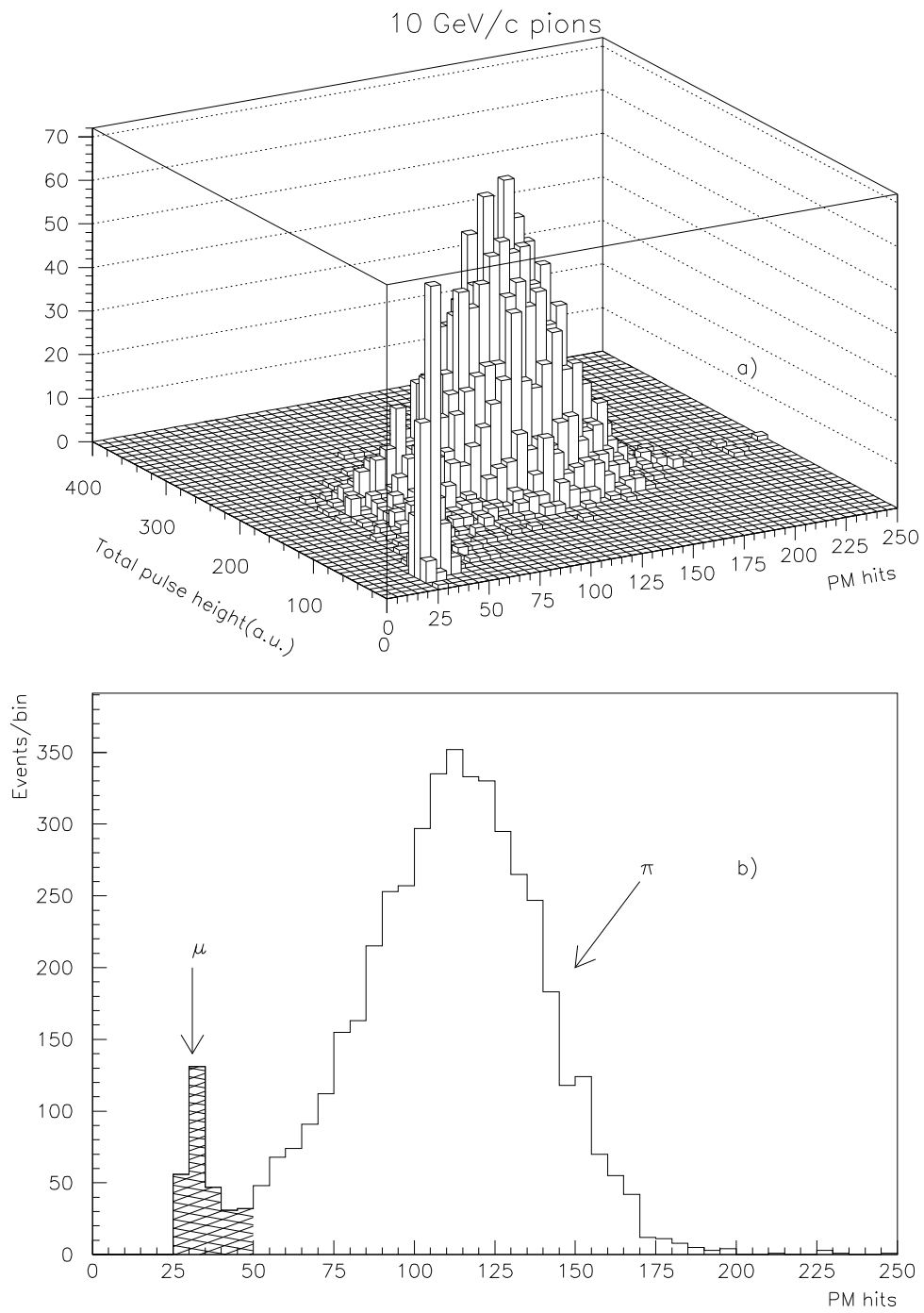
Figure 5: (a) Lego plot of the total number of active PMs versus the total calorimeter pulse-height; (b) projection: the total number of active PMs.

The analog signal of the 1256 photomultipliers of the calorimeter was digitized by dual-range 8-bit ADCs. The nominal ratio of the conversion factors for the two ADCs (high/low sensitivity) was set to 20 for all the channels: the actual value of this ratio for each ADC was determined experimentally by means of cosmic ray events. The ADC integration gate was 220 ns long, enough to contain the pion signal tails. We also took some data with a longer gate (300 ns); no difference was found in terms of calorimeter performance (linearity and energy resolution).

In order to study in more detail the stability and the uniformity of response, a further beam test was performed in April 1995 in the same location and with a similar set-up. For this purpose, an additional fiber detector, lent to us and set-up by the FAROS Collaboration [5], was used to define the beam impact point on the calorimeter with good space accuracy (~ 1 mm).

5. Signal equalization and sector intercalibration

Three sequential steps are needed for the determination of the calorimeter response: first, within each sector, the *equalization* of the signals from each individual PM; then the *intercalibration* between different sectors; and, finally, the overall energy calibration.

The *equalization* of signals from modules of the same type is performed by means of penetrating cosmic rays. An *equalization* constant is computed for each PM by selecting cosmic muons crossing the central region of the modules (± 10 cm), and correcting for the effective track length.

The number of collected cosmic events is large enough to keep the statistical error on each equalization constant at the $\pm 5\%$ level. Systematic effects due to the time dependence of the PM gain and to the position dependence of the energy spectra for the selected muons were also studied, the latter being due to the variable amount of material crossed by the muons before entering the module. The two effects combined account for less than 3% of the total uncertainty.

A typical pulse-height distribution of one module, for example of the HAD1 sector, is shown in Fig. 6a. A similar shape is obtained by summing the signals of all the modules of HAD1 after calibration; no significant widening of the curve is observed (Fig. 6b), thus giving us confidence in the reliability of the method.

To combine the signals of the three different sectors, two *intercalibration* constants are needed, namely those of HAD1 and HAD2 relative to EM. These constants are determined experimentally using pions interacting at different calorimeter depths.
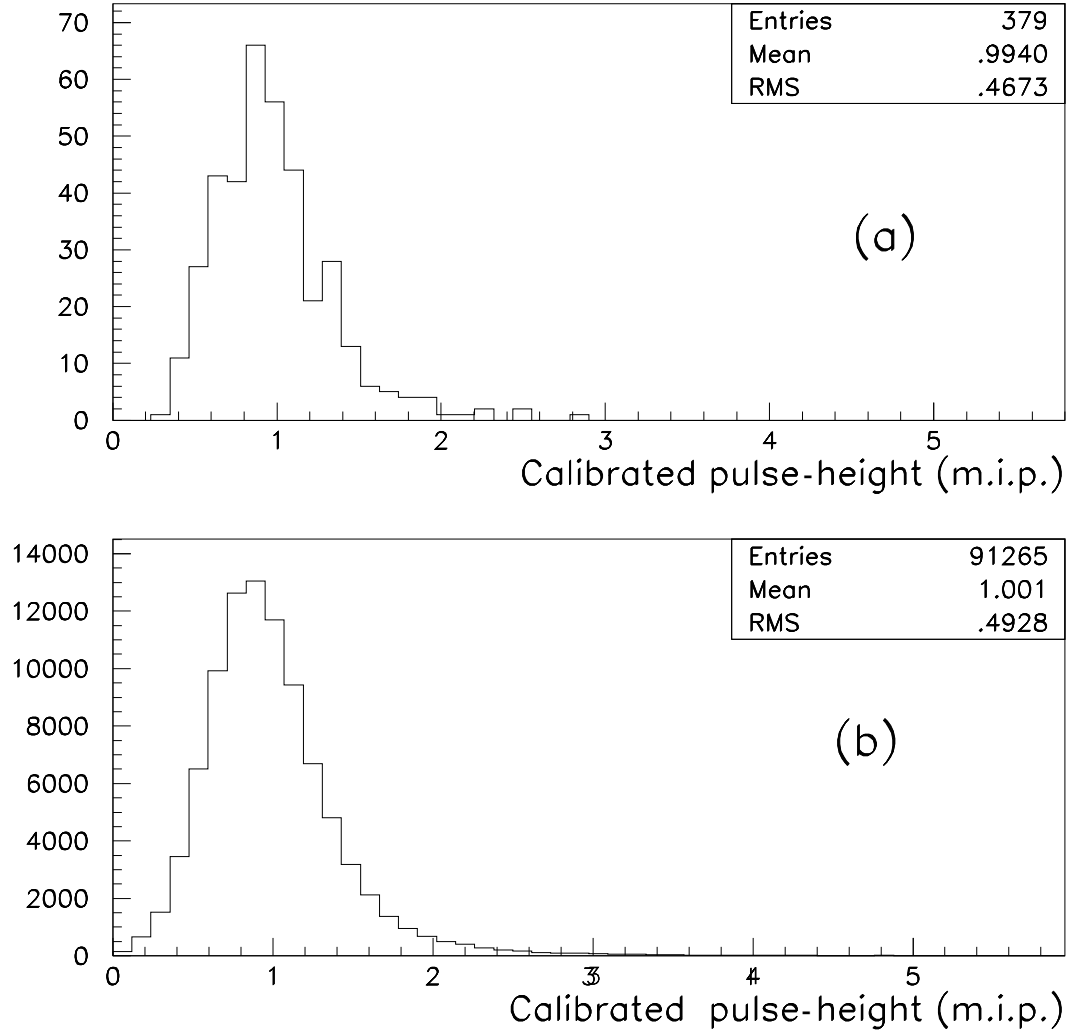
Figure 6: (a) Typical signal distribution induced by cosmic rays in a HAD1 module; (b) the same distribution for the whole HAD1 sector.

Given that the response of each sector to a certain amount of deposited energy must be the same, one can select events where the shower is fully contained in two consecutive sectors A and B; therefore, the energy responses of A and B (S_A, S_B) are related to the relative intercalibration factor $\alpha_{B,A}$ by the linear equation

$$S_A + \alpha_{B,A} S_B = E_{\text{shower}} \ .$$

E_{shower} is the shower energy, related to the pion energy by the relation

$$E_{\text{shower}} = E_\pi - \frac{\mathrm{d}E}{\mathrm{d}x} \, \Delta X \ ,$$

9

which implies a correction for the pion energy loss before interacting at the depth ΔX. In Fig. 7 we show, as an example, S_{HAD1} as a function of S_{HAD2} for pions of a given momentum interacting at different depths. A linear fit to the points allows the constant of calibration between the two sectors to be determined. This procedure is repeated for several beam momenta. As expected, the parameters of the fit are, within the errors, independent of the pion energy.
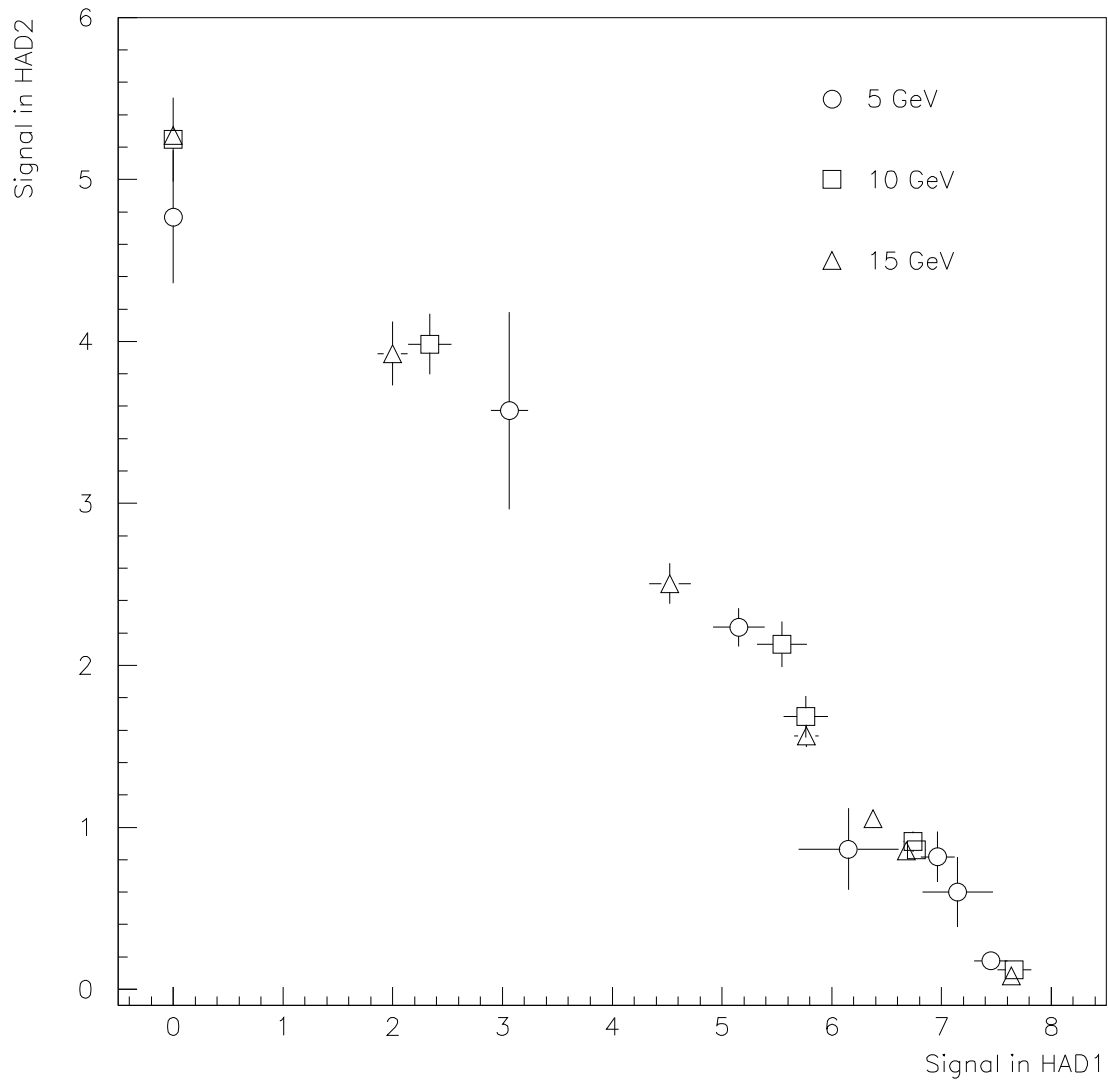
Figure 7: Energy deposited in HAD2 as a function of the energy deposited in HAD1 by 5, 10 and 15 GeV/c pions interacting at different depths in the calorimeter. A straight line fit to the points allows the intercalibration constant between the two sectors to be determined.

10

With this method we can determine directly

$$\alpha_{\mathrm{HAD1,EM}} = 2.34 \pm 0.06$$

and

$$\alpha_{\mathrm{HAD2,HAD1}} = 1.40 \pm 0.02 \; ,$$

which leads to

$$\alpha_{\mathrm{HAD2,EM}} = 3.28 \pm 0.10 \; .$$

It turns out that compatible numbers may be obtained by minimizing the energy resolution for pion-induced showers, but the approach described was preferred to avoid any bias.

It should be noted that the mean thicknesses of active material along the beam direction for HAD1 and HAD2, normalized to the EM value (2.1 and 2.5), do not account for the different geometries and sampling frequencies. Therefore, these values are not expected to be appropriate as *intercalibration* constants for (hadron) showers.

6. The calorimeter signal

The calorimeter response to the incoming particle(s) is determined by adding up the energy deposited in all the modules once the *equalization* and *intercalibration* procedures described in Section 5 have been performed. As noted before, each read-out cell is equipped with a PM at each fiber (strip) end, in order to reduce the influence of the light attenuation in the scintillator. This leads to different possible definitions of the module signal, according to the way the two PM signals (L and R) are combined. In particular, one can use the arithmetic or the geometric mean:

$$S_{\mathrm{a}} = \frac{S_{\mathrm{L}} + S_{\mathrm{R}}}{2} \; , \qquad S_{\mathrm{g}} = \sqrt{S_{\mathrm{L}} \times S_{\mathrm{R}}} \; .$$

Under the assumption of a single hit per module and exponential light attenuation in the fibers (strips), as found in Ref. [2], the geometric mean yields a value for the module response (and hence for the energy) which is independent of the hit position x along the module with length L :

$$S_{\mathrm{L}} = A e^{-(x/\lambda)} \; , \qquad S_{\mathrm{R}} = A e^{-(L-x/\lambda)} \; \rightarrow \; S_{\mathrm{g}} = A e^{-(L/2\lambda)}$$

A small position dependence arises in the case of multiple hits.

A correction must be applied for the channels which are noisy or dead. The signal of the other PM of the same cell is used in this case, after correction for the light attenuation corresponding to the hit position. During the beam-test data-taking, only about 10 channels needed this correction.

In Fig. 8 we show the calorimeter signal distribution produced by 10 GeV/c negative pions. Each entry corresponds to the calibrated sum of the response of all the modules, as obtained in calculating the geometric mean. The shape is Gaussian, indicating that both the *calibration* and *intercalibration* procedures do not introduce any appreciable bias in the determination of the overall calorimeter response. All the results presented in this paper were obtained following the same described procedure.
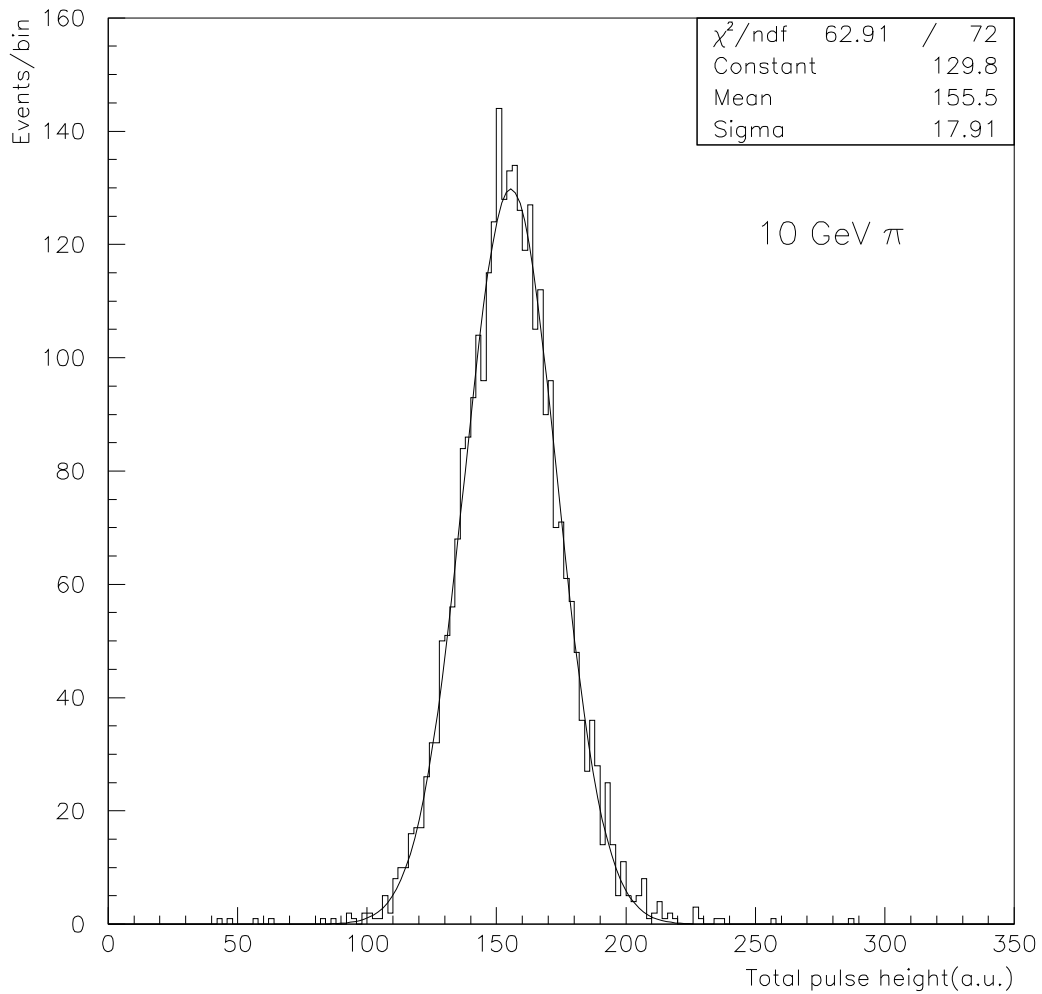
Figure 8: Calorimeter response to 10 GeV/c pions.

7. Monte Carlo simulation

A Monte Carlo simulation of the calorimeter was performed in order to study its response to different kinds of incoming particle and to showers initiated by neutrino interactions. Calorimeter behaviour was simulated by reproducing the full geometry, down to the details of the scintillating fiber (strip) and lead structure of the different modules. Direct tracking of charged and neutral particles is performed, including all types of secondaries, down to at least 10 keV. All electromagnetic and hadronic processes (elastic and inelastic) are taken into account.

The task was accomplished by using the GEANT 3.21 package [6], together with FLUKA [7] for the hadronic reactions, and MICAP [8] to deal with low energy (20 MeV) neutron interactions down to the thermal region of a few eV kinetic energy. Many other effects related to the actual digitization and read-out of the calorimeter are included:

- Birk's law related to the light yield of the scintillator;

- the attenuation length of the light in the scintillator simulated using the experimental values for the different types of module;

- the signal resolution, parametrized according to

$$\frac{\sigma(s)}{s} = \sqrt{\frac{\alpha}{s} + \beta} \ ,$$

  where s is the light intensity at the photocathode. The constants α and β are determined experimentally by comparing the output of the two PMs connected to the same module. The first term under the square root represents the photoelectron statistics, while β, found to be negligible, includes all the imperfections in the light collection:

- the actual ADC time integration gate (220 ns) is used to cut the tails of the thermal neutron energy deposition;

- the dual range ADC digitization is reproduced as in the real case.

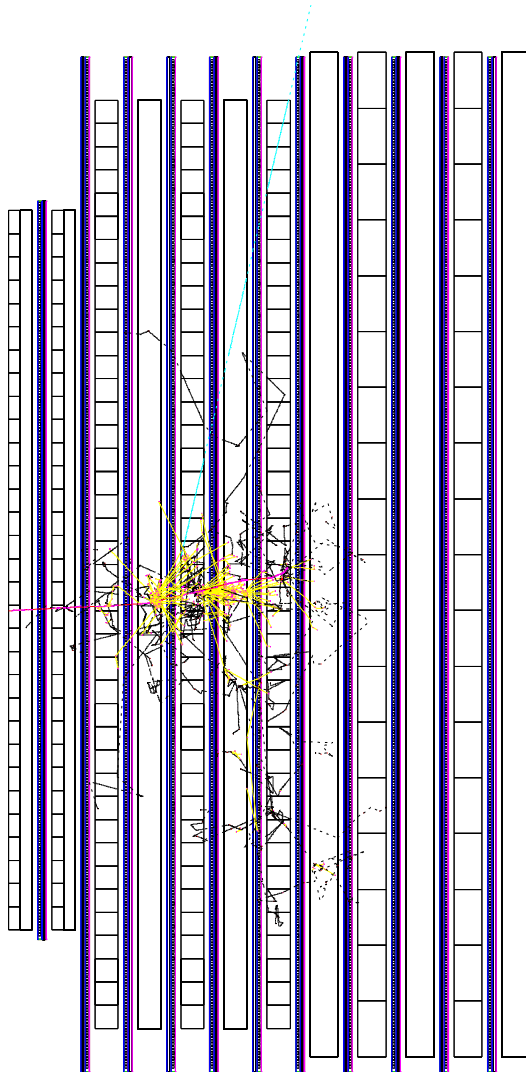Figure 9 shows a typical Monte Carlo event induced by a 3 GeV/c pion.

Figure 9: Monte Carlo simulation of a 3 GeV/c pion event; solid and dashed lines represent charged and neutral particles, respectively.

8. Response to electrons

The electron response was studied for different SPS beam momenta, in the range from 2.5 to 10 GeV/c, relevant for the CHORUS experiment. For each momentum, a Gaussian fit was performed to the distribution of the calorimeter signal (Fig. 10), as defined in Section 6. The mean value S of the Gaussian is plotted against the beam momentum P Fig. 11.
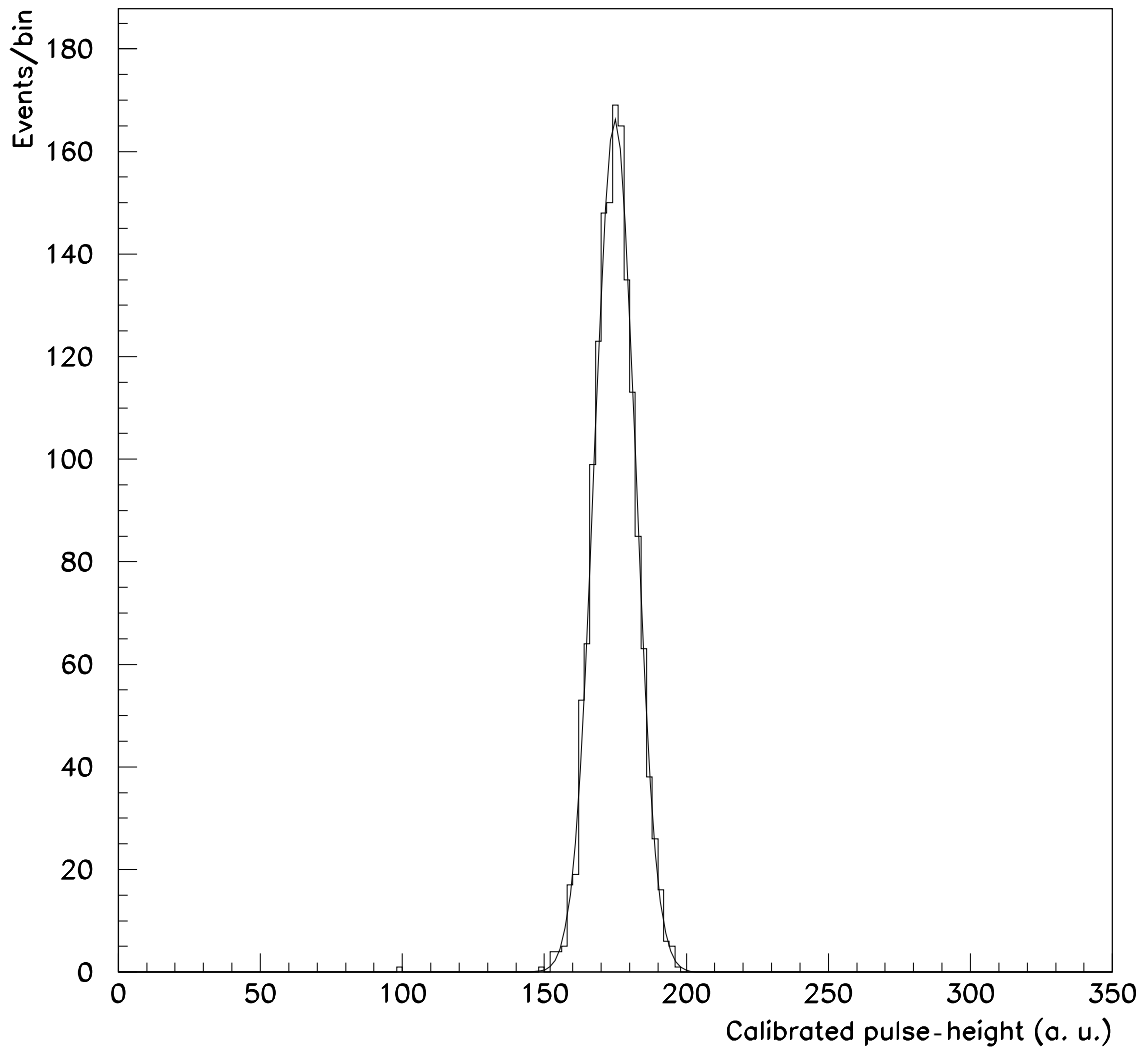
Figure 10: Calorimeter response to 10 GeV/c electrons.
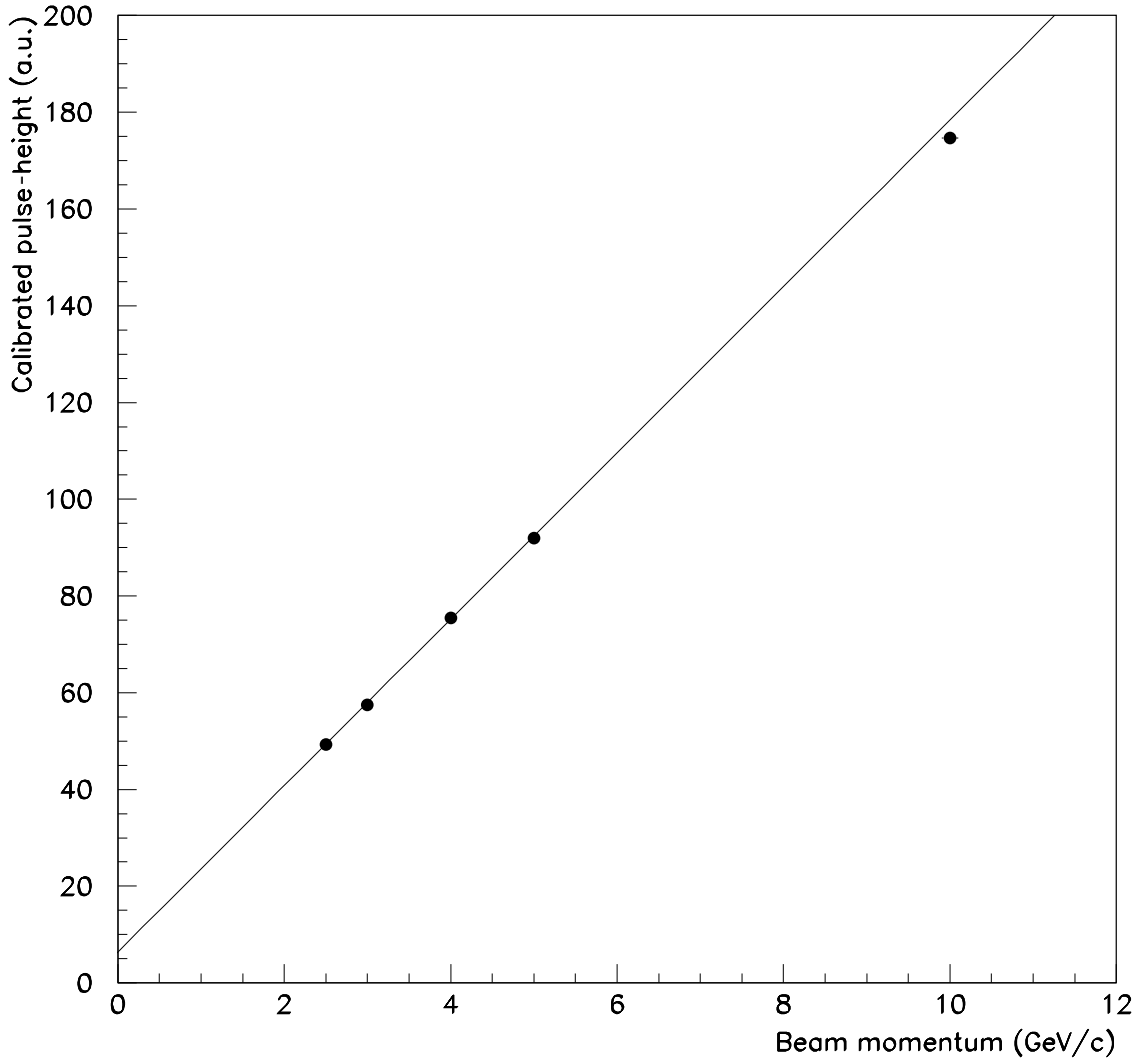
Figure 11: Calorimeter response as a function of the electron momentum.

The measured points lie on a straight line up to 10 GeV/c, where electronics saturation tends to reduce the calorimeter signal. This effect is due to the small spatial dimensions of the electromagnetic showers, such that a large fraction of the energy can be released in a single EM module. This does not happen for hadron- or neutrino-induced events, where many modules share the incident energy.

The result of a linear fit (also shown in Fig. 11) performed in the interval from 2.5 to 5 GeV/c indicates that extrapolation to zero pulse-height leads to a *negative* value of the momentum:

$$S \;=\; (17.2 \pm 0.3) \;\times P(\mathrm{GeV}/c) \;+\; (6.4 \pm 0.9) \;.$$

The above result is in agreement with our previous analysis on the electromagnetic response of single calorimeter modules, tested on the same beam line [2]. It is consistent with the actual value of the beam momentum being 370 ± 50 MeV/c higher than the nominal value.

The electromagnetic response of the calorimeter and its linearity have been thoroughly investigated by simulation. Monte Carlo predictions give a linear response of the detector to electrons, as well as to photons, and no offset is expected. As pointed out in [2], the source of this experimental offset may depend upon the SPS beam momentum calibration.

In order to solve this problem, independent measurements were carried out at the CERN PS. A set-up consisting of 4 EM and 1 HAD1 modules, able to contain electromagnetic showers, was exposed to low-momentum electrons (1–7 GeV/c) from the T11 beam. The results indicate that the extrapolation to zero calorimeter pulse-height does indeed lead to a momentum compatible with zero (intercept equal to $+40 \pm 20$ MeV/c), supporting the conclusion of a calibration shift of the SPS X9 beam momentum. These results are shown in Fig. 12, together with the SPS points corrected for the 370 MeV/c offset. The agreement between the two sets of data is excellent.
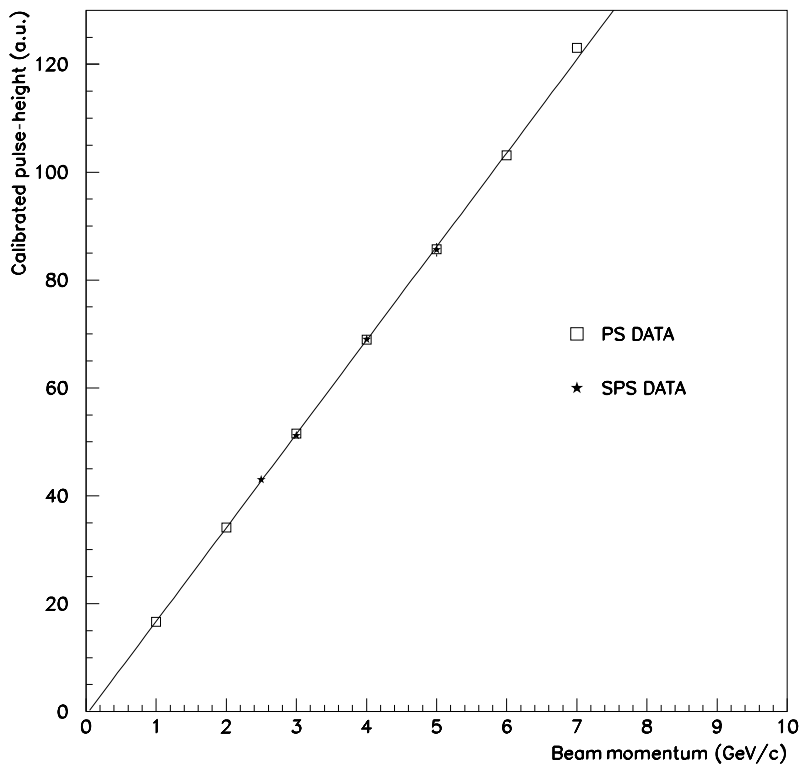
Figure 12: Electron response for the PS set-up. The SPS points are also shown, corrected for the 370 MeV/c momentum shift.

17

The following (corrected) relation is then obtained for the energy dependence of the electromagnetic response:

$$S = (17.2 \pm 0.3) \times P(\text{GeV}/c) - (0.14 \pm 0.96) \ . \tag{1}$$

The energy resolution $\sigma(E)/E$ is plotted in Fig. 13 as a function of the electron energy. The energy dependence of the resolution is well fitted by the usual function:

$$\frac{\sigma(E)}{E} = \frac{(13.8 \pm 0.9)\%}{\sqrt{E(\text{GeV})}} + (-0.2 \pm 0.4)\% \ .$$

This result fulfils the design requirements and agrees with the Monte Carlo predictions.
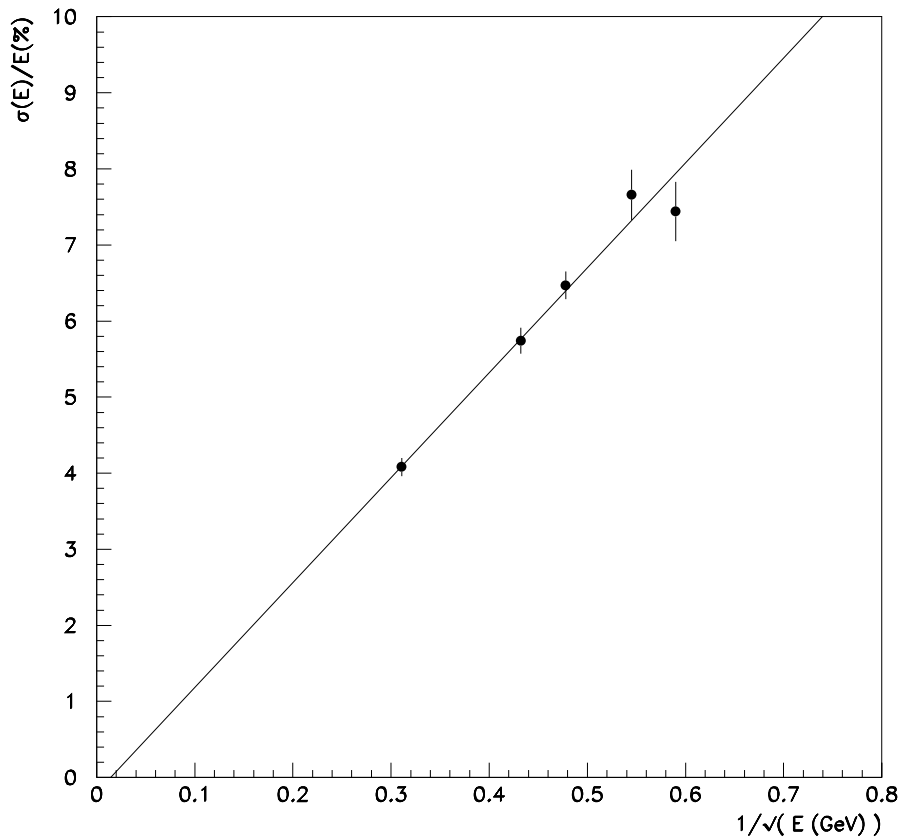
Figure 13: Energy resolution for electrons as a function of the energy.

We also studied the uniformity of the electromagnetic response as a function of the particle impact point on the calorimeter. Given the very limited transverse dimensions of electromagnetic showers in a lead calorimeter, we expect a reduction of the signal response to occur near the EM module edge, where no active material is present (crack).

For this analysis we used the FAROS detector to select electrons hitting the calorimeter in the crack between two adjacent (vertical) modules in the second EM plane, where showers are already developed. Figure 14a shows the total energy
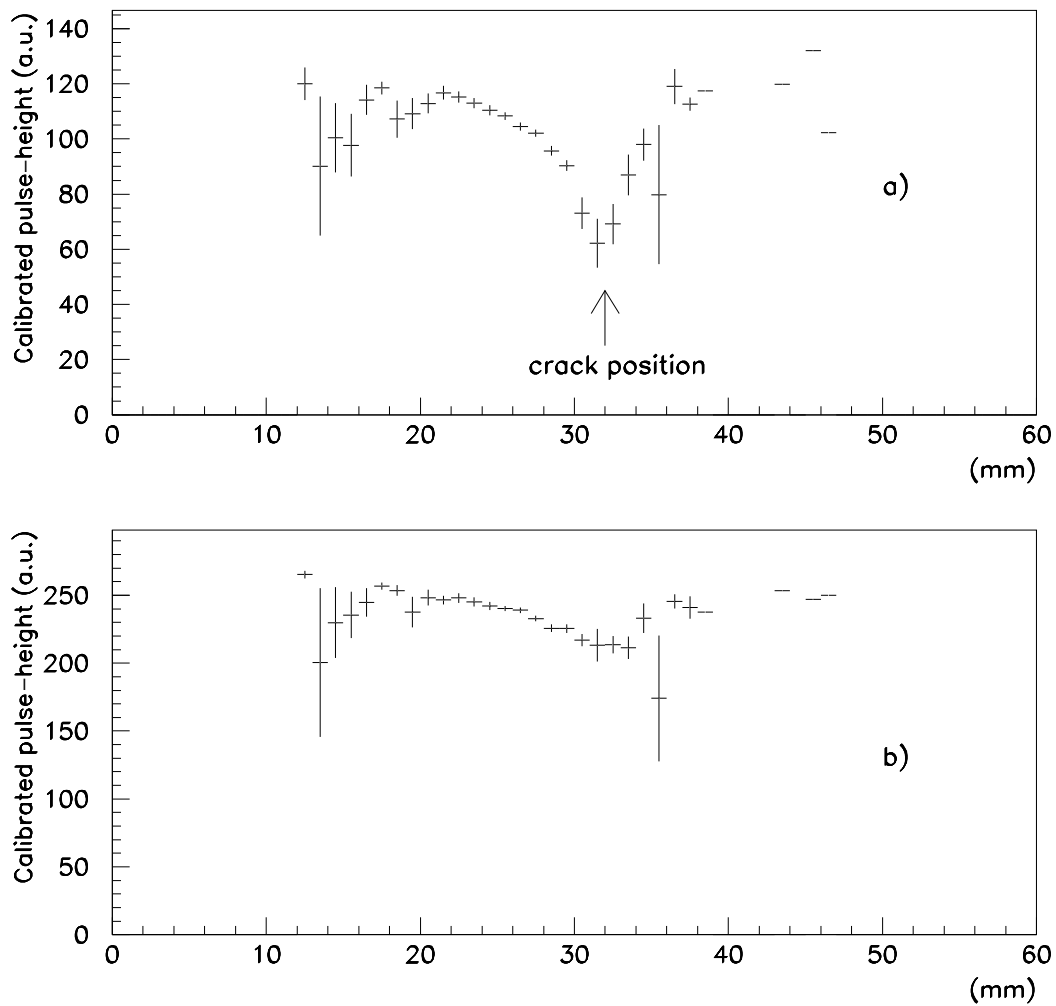
Figure 14: (a) Energy deposition in the second EM plane as a function of the horizontal beam impact-point, for 10 GeV/c electrons. The dip corresponds to the boundary between two vertical modules; (b) the corresponding total calorimeter signal as a function of the impact point.

19

released in that plane, by 10 GeV/c electrons, as a function of the impact-point horizontal coordinate. One can see that, in a region 4 mm wide centred on the crack, the signal is reduced by about $25 \div 40\%$, indicating that part of the shower energy is, in this case, undetected. The consequent reduction in the total calorimeter signal amounts to $5 \div 10\%$, as shown in Fig. 14b. However, applying geometrical considerations, this disuniformity would affect, on average, only 2% of the electromagnetic showers. We did not use events occurring in the crack in previous studies on the electromagnetic response and energy resolution.

By studying electron showers developing in different calorimeter zones we estimated the disuniformity in the electromagnetic response to be of the order of $\pm 5\%$, in agreement with the design requirements.

9. Response to pions

In the following analysis, to study the hadronic performance of the calorimeter without systematic errors caused by showers leaking at the rear of the detector, we selected only those events with the pion interacting in the EM section.

The pion response was studied for different beam momenta, from 3 to 20 GeV/c. The mean value S of the signal distribution, which is Gaussian as in the electron case, is plotted in Fig. 15 as a function of the nominal momentum P, corrected for the shift of 370 MeV/c, found with the electron data. The measured pion momentum-dependence may be parametrized as:

$$S = (15.3 \pm 0.2) \times P(\text{GeV}/c) - (5.8 \pm 1.0) , \tag{2}$$

which corresponds to a *positive* intercept of 380 ± 65 MeV/c. A different value of this quantity is expected for electrons (compatible with zero) and pions, which can be understood on the basis of the following considerations:

– A comparison of the response to electrons and pions of the same energy shows deviations from exact compensation ($S_{\text{electron}} > S_{\text{pion}}$). Therefore, at high momenta, the increase in the electromagnetic energy content in the hadron showers [$\frac{E_{\text{EM}}}{E_{\text{TOT}}} \propto \ln(E_{\text{TOT}})$] induces an energy-dependent enhancement of the signal.

– At low momenta (~ 1 GeV/c), the contribution from neutral pions becomes negligible and small multiplicity processes dominate. In this case, the effect of the particle masses not converted into visible energy in the read-out gate becomes visible.
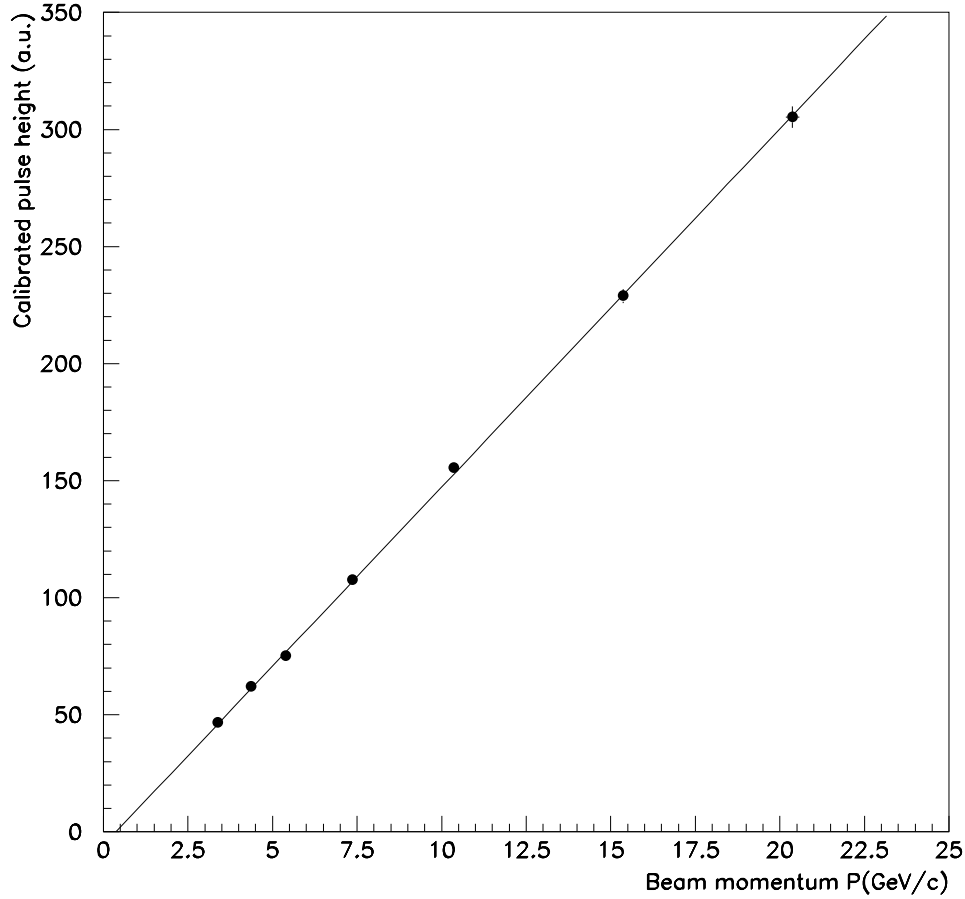
Figure 15: Calorimeter response as a function of the pion momentum.

Both the above effects indicate that a straight-line fit to the data taken in the stated momentum range should have an intercept at a positive value of the abscissa. This is confirmed by the Monte Carlo simulation, which predicts an intercept of 340 ± 50 MeV/c. From Fig. 16, where the response per unit energy is plotted as a function of the pion momentum, one finds that the calorimeter is linear within 2% in the range 3 to 20 GeV/c and that there is no evidence for saturation, even at the highest energy.
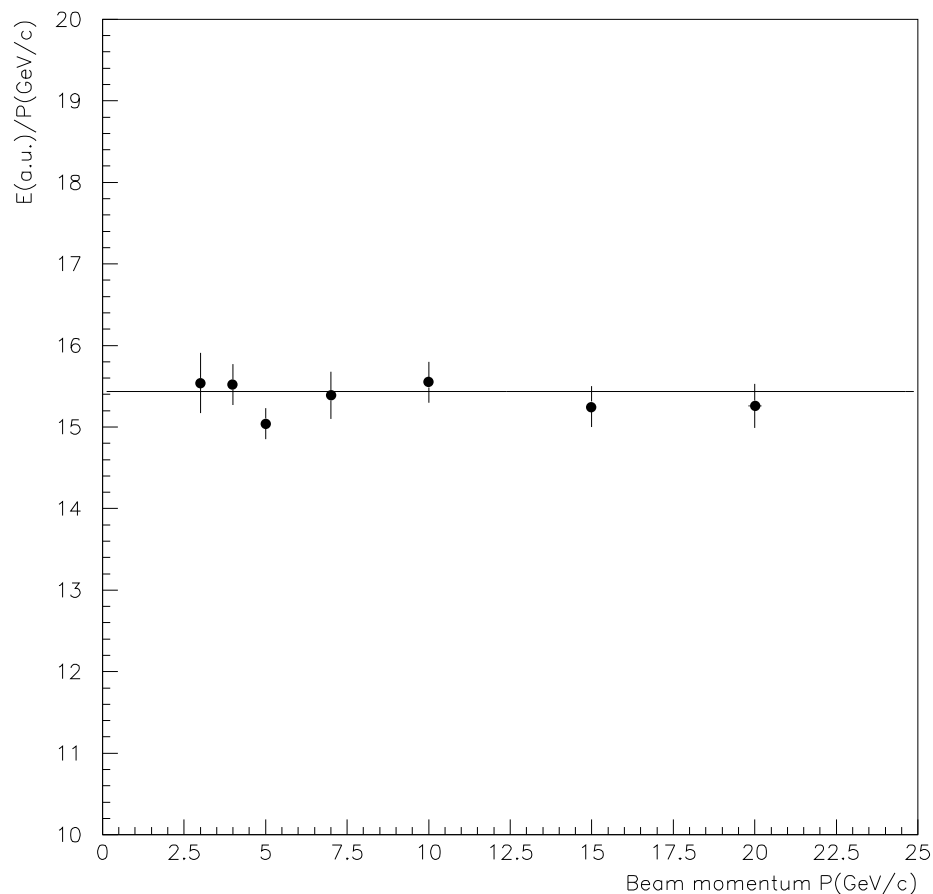
Figure 16: Calorimeter response per unit momentum as a function of the pion momentum.

In conclusion, the SPS pion/electron linearity measurements are internally consistent and in agreement with the simulation, within the hypothesis of an offset in the nominal beam momentum.

From the Gaussian fit to the response distributions one determines the energy resolution $\sigma(E)/E$, which is plotted in Fig. 17 as a function of the pion energy. The errors assigned to each point include a systematic uncertainty of about 2%, determined by applying different event selection criteria to the data, and by studying pions hitting different calorimeter positions. The above uncertainty is lower than that for the electron case ($\pm 5\%$). The main reason for this is that more calorimeter modules are involved in a hadron shower. Note that a study performed with the FAROS detector, similar to the case of electrons, does not show, as expected, any *crack* effect. The energy dependence of the resolution is parametrized as:

$$\frac{\sigma(E)}{E} = \frac{(32.3 \pm 2.4)\%}{\sqrt{E(\text{GeV})}} + (1.4 \pm 0.7)\%$$

The predictions of a Monte Carlo simulation are also shown in Fig. 17.
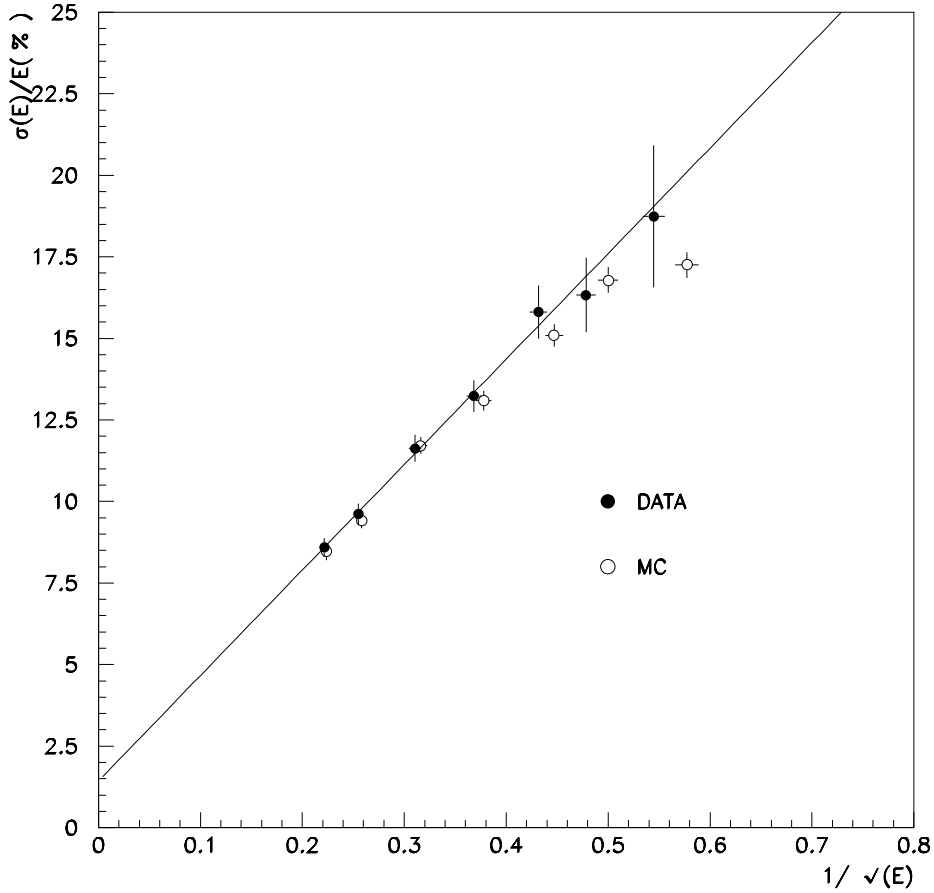
Figure 17: Pion energy resolution as a function of the energy. The open circles show the Monte Carlo predictions.

The experimental energy resolution can be interpreted in terms of the different energy resolutions of the fiber and strip sectors:

$$\frac{\sigma(E)}{E} = \sqrt{k(\sigma_f/E)^2 + (1-k)(\sigma_s/E)^2} \; ,$$

23

where k is the measured energy fraction in the fibers sector (0.89 at 10 GeV) and σ_f/E is its expected resolution ($30\%/\sqrt{E}+0.5\%$), while σ_s/E is the resolution of the strip calorimeter alone. As an example, the above formula yields, for the experimental resolution of 11.6% at 10 GeV, an energy resolution of $60\%/\sqrt{E}$ for the HAD2 calorimeter.

The longitudinal and transverse shower development in the calorimeter is shown in Fig. 18 for a 10 GeV/c pion. Many events are superimposed to obtain the *average* behaviour. Figure 19a shows the projection of the shower onto the transverse plane. In Fig. 19b it is shown that a cylinder containing 95% of the shower energy has a radius of about 25 cm, almost constant in the energy range explored by our measurements. This result is in excellent agreement with the Monte Carlo prediction, also shown in the figure.
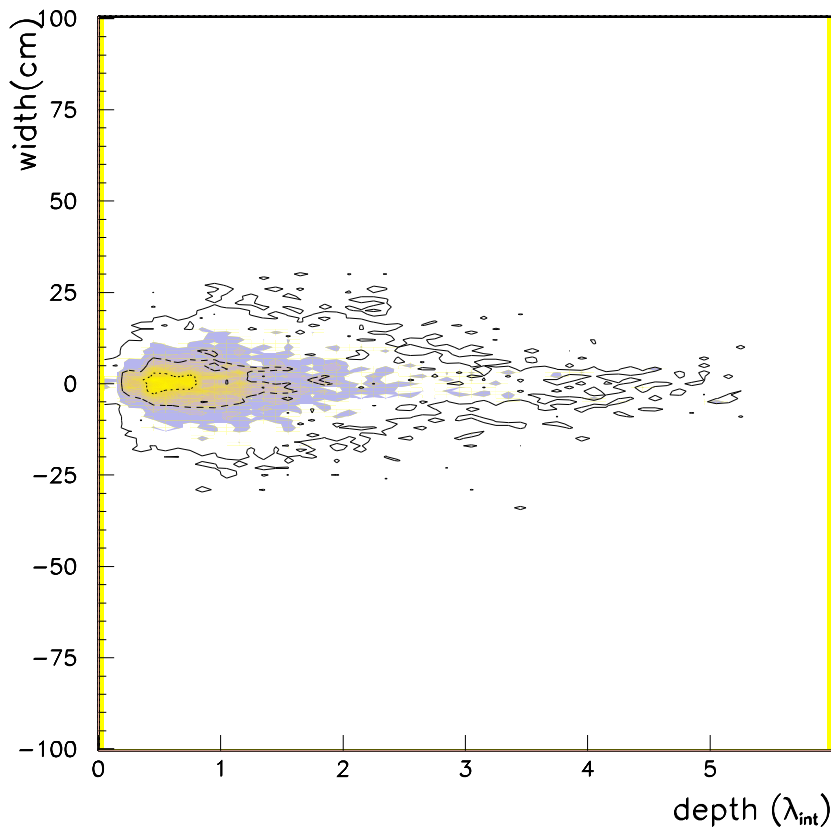
Figure 18: Shower development for 10 GeV/c pions. Different grey zones correspond to different pulse-height levels. The continuous line is 1% of the maximum intensity.

24
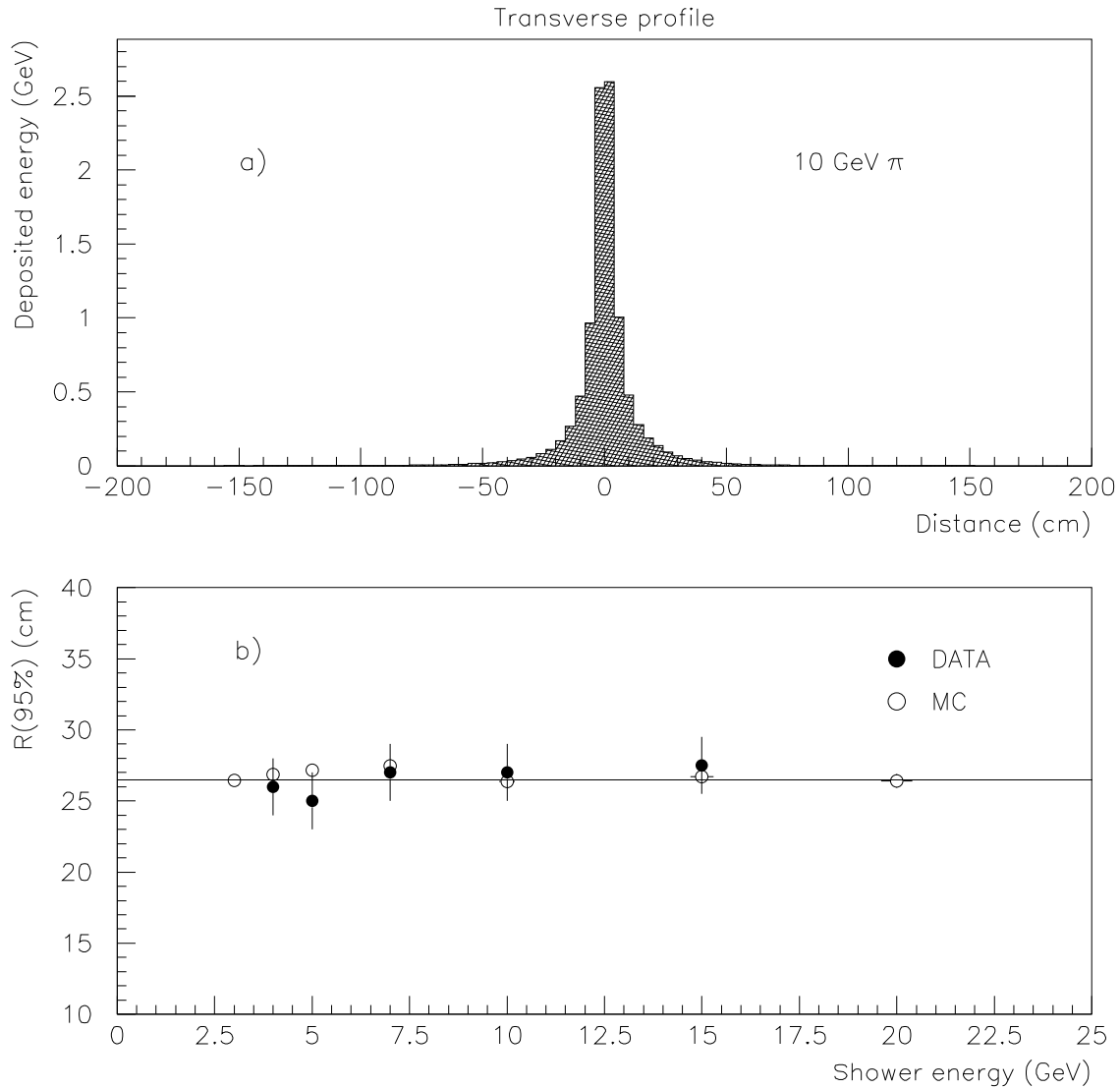
Figure 19: (a) Shower projection onto the transverse plane orthogonal to the beam direction for 10 GeV/c pions; (b) transverse dimensions of the pion shower as a function of the energy: the black circles represent the radius around the shower axis which contains 95% of the energy. The open circles show the Monte Carlo predictions.

The longitudinal development is presented in Fig. 20a for different pion momenta. Figure 20b shows the fraction of energy deposited at different calorimeter depths normalized to the total calorimeter signal. In both cases, the Monte Carlo results are also given; the comparison indicates very good agreement.
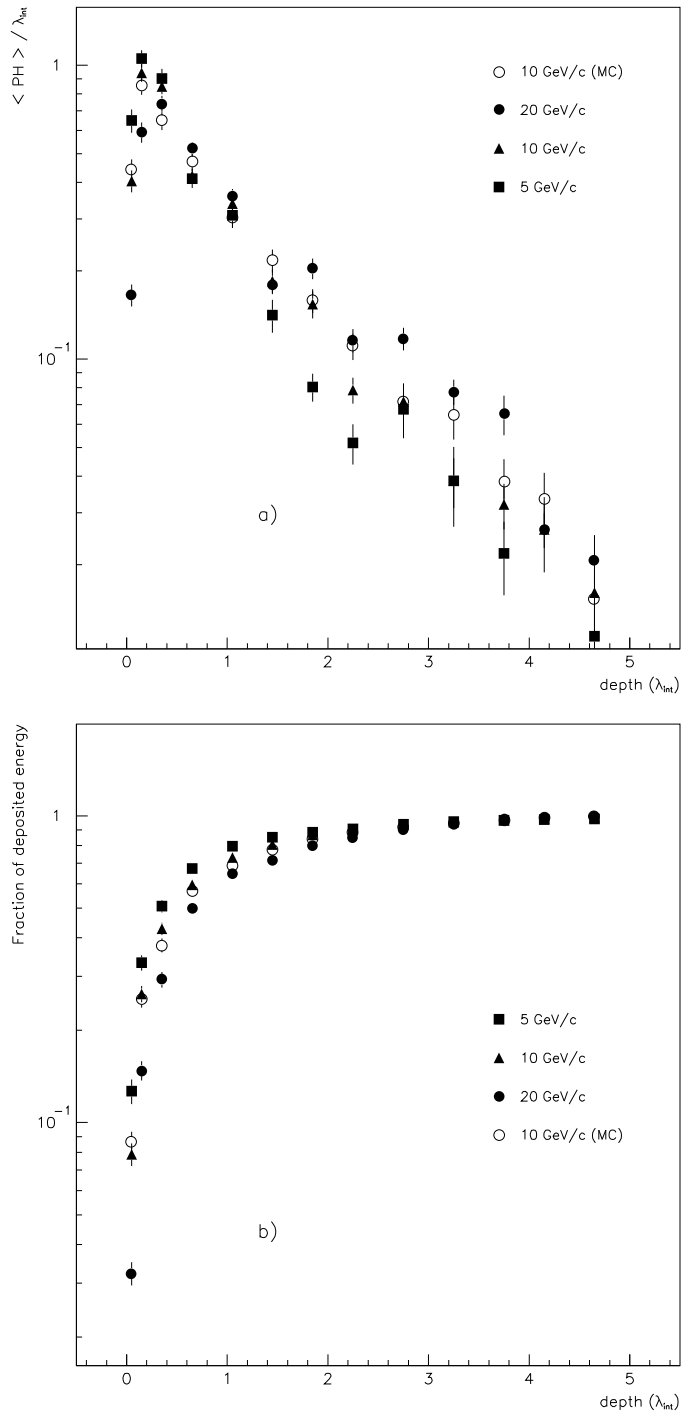
Figure 20: (a) Longitudinal shower development for different pion momenta; (b) fractional energy deposition. The Monte Carlo simulation result is also shown for 10 GeV pions.

We also studied the calorimeter performance for measurement of the shower direction. The angular resolution is determined using the centre of gravity of the energy deposition in each calorimeter plane. Figures 22a and 22b show, respectively for the two projections (the beam goes along x), the energy centre of gravity distributions (per plane), induced by 10 GeV/c pions. From a knowledge of the centre of gravity coordinates in the different planes, event by event, one can determine the shower direction. The distributions of the fitted angle for both projections are shown in Figs. 21a and 21b for 10 GeV/c pions. We obtained an angular resolution of about 60 mrad (HWHM) at 10 GeV/c for the two transverse projections. The effect of the beam angular-spread (< 1 mrad), folded into the measurement, can be neglected. The Monte Carlo predictions, shown in the figure, are in agreement with the data[3].
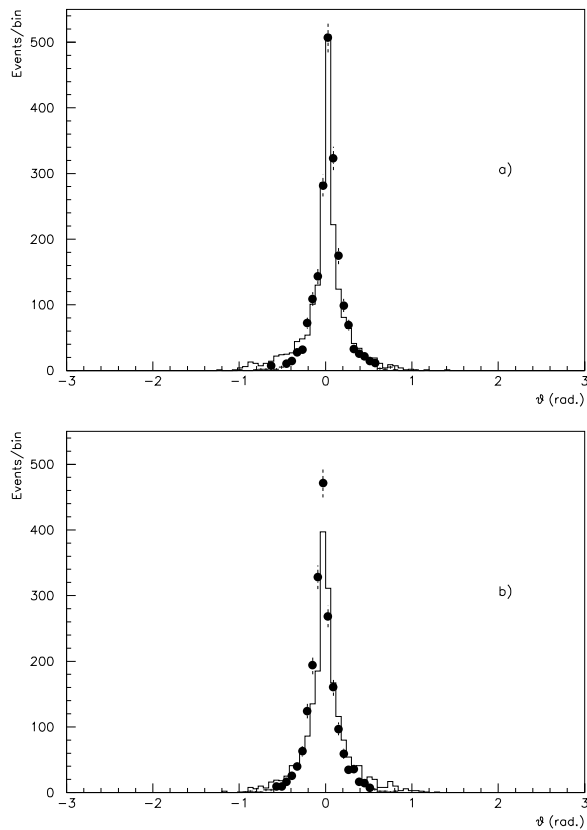
Figure 21: Angular resolution for 10 GeV/c pions: (a) x–z projection, (b) x–y projection. The continuous line represents data events and the black circles show the results of Monte Carlo simulation.

---

[3]A better angular resolution was obtained in CHORUS using the calorimeter information and the position of the neutrino interaction point in the emulsion target [3].
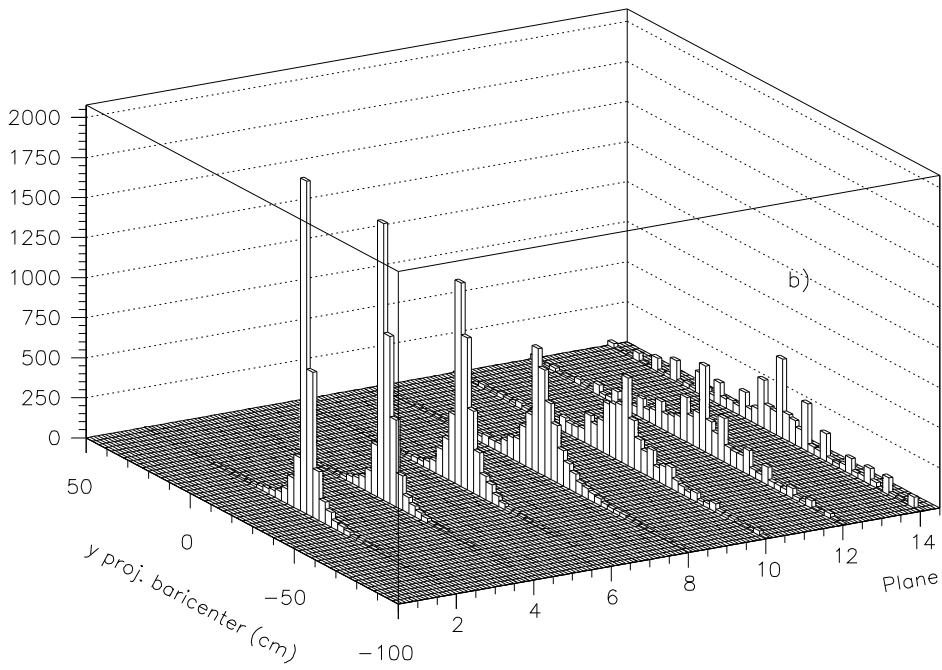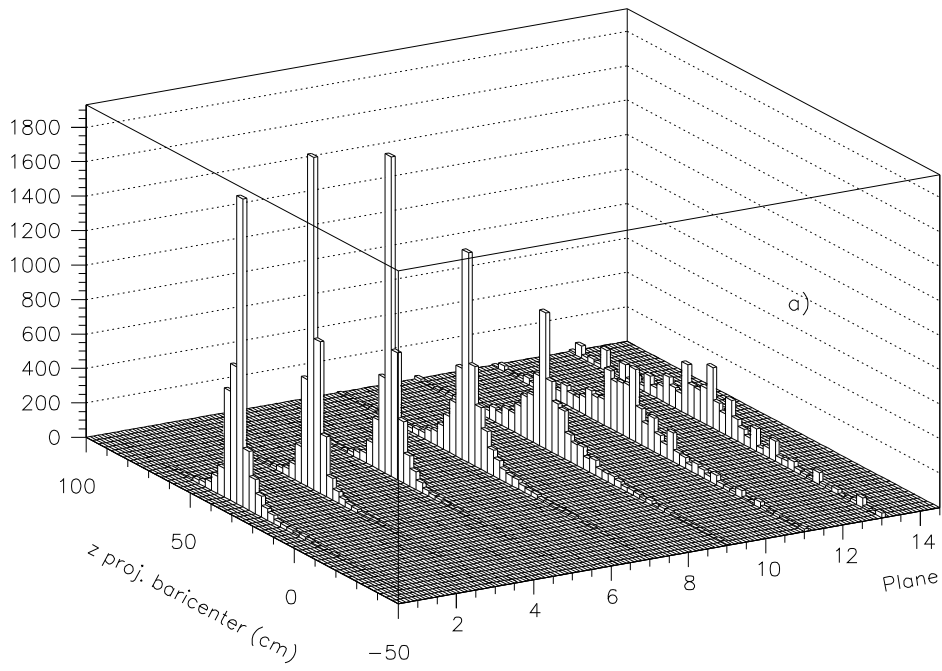
Figure 22: Energy centre of gravity distributions (per plane) induced by 10 GeV/c pions; (a) x–z projection (b) x–y projection.

From the electron and pion response of the calorimeter we can determine the experimental e/π ratio. In Fig. 23 we plot the ratio of the average electron and pion calorimeter signal, calculated at the same (corrected) momentum, as a function of the momentum. The systematic error, due to the response disuniformity, has been added to the statistical error. In the same figure, we plot the ratio of the functions (1) and (2), describing the signal momentum dependence for electrons and pions. This measurement, performed at relatively low energy, does not allow us to calculate the e/h ratio, where h is defined as the purely non-electromagnetic component of the hadron shower.
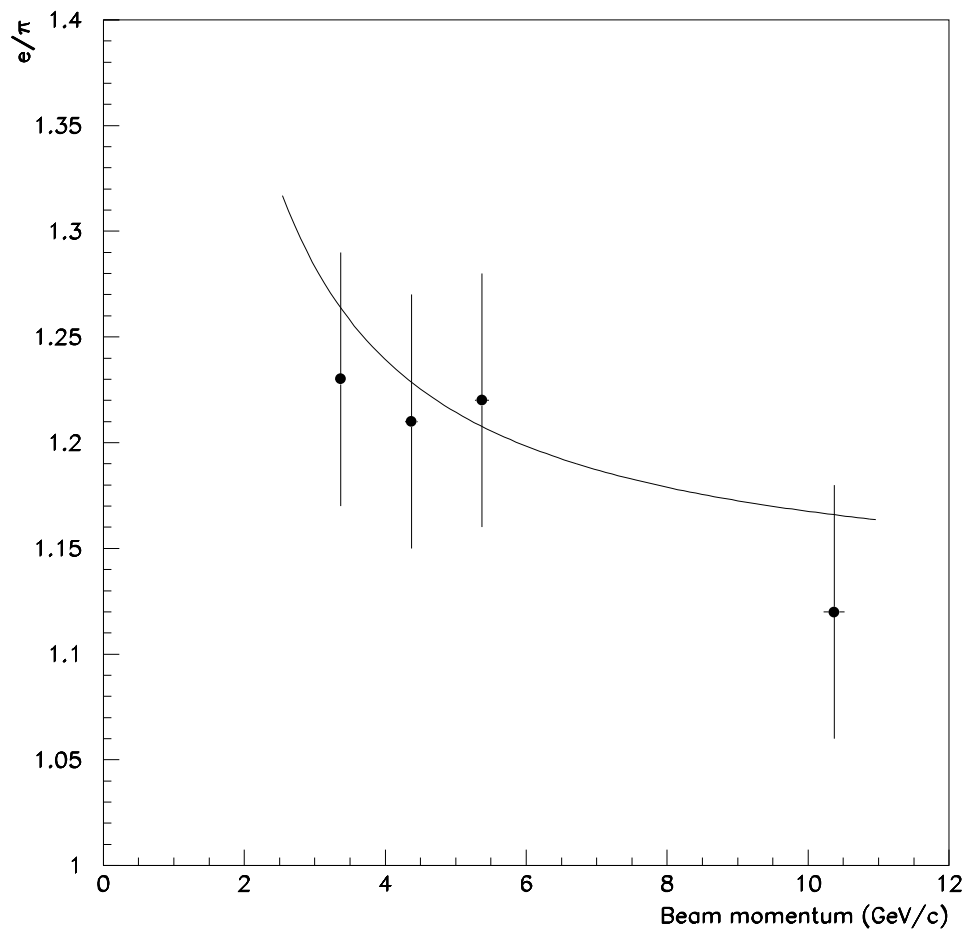
Figure 23: e/π ratio as a function of the beam momentum. The continuous line represents the ratio of the electron and pion momentum-dependence functions.

10. Conclusions

We have presented experimental results on the electron and pion response of the calorimeter for the CHORUS experiment. The calorimeter, the first large-scale application of the scintillating-fiber/lead technique for integrated electromagnetic/hadronic calorimetry, was exposed to electron and pion beams in the momentum range 2.5 to 20 GeV/c at the CERN SPS. A further test of calorimeter modules, performed at the CERN PS, allowed us to study the low-energy electromagnetic response.

Electrons were studied, in the SPS beam, in the momentum range 2.5 to 10 GeV/c. The calorimeter response was found to be linear with the momentum after applying a correction to its nominal value, as indicated by measurements performed at the CERN PS. The energy dependence of the resolution was parametrized as $\sigma(E)/E = (13.8 \pm 0.9)\%/\sqrt{E(\text{GeV})} + (-0.2 \pm 0.4)\%$.

The calorimeter response to pions was linear in the momentum range explored by the measurements, and we achieved an energy resolution of $\sigma(E)/E = (32.3 \pm 2.4)\%/\sqrt{E(\text{GeV})} + (1.4 \pm 0.7)\%$. This result is in agreement with the design features and the Monte Carlo predictions.

The shower development, in the longitudinal and transverse directions was studied as a function of the beam momentum and the results obtained are in good agreement with the Monte Carlo expectations. The comparison between the pion and electron response allowed us to measure the e/π ratio in the low-momentum region.

The calorimeter has been successfully operational during the 1994 and 1995 data-taking periods of the CHORUS experiments in the CERN Wide Band Neutrino Beam.

References

[1] D. Acosta et al., Nucl. Instrum. Methods **A308** (1991) 481.

[2] S. Buontempo et al., Nucl. Instrum. Methods **A349** (1994) 70.

[3] M. de Jong et al., CERN–PPE/93–131.

[4] Particle Data Group, Phys. Lett. **B239** (1990), page III 5,6.

[5] V. Agoritzas et al., LAPP–EXP–95–01, Proc. Int. Conference on Advanced Technology and Particle Physics, Como, 3–7 October 1994.

[6] CERN Program Library Long Writeup Q123.

[7] A. Fassò et al., FLUKA92, Proc. Workshop on Simulating Accelerators Radiation Environments, Santa Fe, 11–15 January 1993.

[8] T.A. Gabriel and J.O. Johnson, Technical Report TM 10340, ORNL.